Kumar and Kumar
Journal of Engineering and Applied Science (2023) 70:117
https://doi.org/10.1186/s44147-023-00289-3

Journal of Engineering and Applied Science

RESEARCH Open Access

Investigation of machining characteristics and surface integrity for trim cut WEDM of hybrid metal matrix composite [Al 6061, SiC, and TiB_2]

Nilesh Kumar[1,2*] and Jatinder Kumar[1]

*Correspondence: nileshmehus@gmail.com

[1] Department of Mechanical Engineering NIT, Kurukshetra, Haryana, India
[2] Indian Air Force, Ambala Cantt, Haryana 133001, India

Abstract

This study is focused on fabrication of Hybrid Al6061/SiC + TiB_2 MMC by stir casting process, primarily to study the effect of two different reinforcement particles on mechanical properties and microstructure. Additionally, the assessment of surface integrity has been attempted after machining the composite by trim cut WEDM process. Five samples have been fabricated with varied weight fraction of SiC and TiB_2 reinforcement, keeping total weight percentage of reinforcement particles fixed to 10%. It is observed that Hybrid MMC with composition Al6061 (90%), SiC (2.5%), and TiB_2 (7.5%) shows better mechanical properties which is corroborated by both the optical microscopy and SEM. A screening experiment has been designed using fold over fractional factorial technique (with resolution IV), to investigate the parametric effects on surface integrity features, i.e., surface roughness, spark gap, and recast layer for trim cut WEDM operation. Peak current (I_p) and pulse on time (T_{on}) have been found to be the significant parameters for spark gap as well as surface roughness. It is observed that the trim cut operation improved the surface roughness and reduced it to 2.2 µm from 3.93 µm (after rough cut). Recast layer has been reduced to a value of 4.67 µm after trim operation, from 24.6 µm for rough cut. These findings suggest that trim cut strategy is very effective in improving the surface integrity of the rough-cut machined samples. It is also observed that thickness of recast layer is directly proportional to the discharge energy during trim cutting.

Keywords: Stir casting, Hybrid MMC, Fold over fractional factorial design, Trim cutting, WEDM, Optical microscopy, SEM, Recast layer

Introduction

The composites emerged as a distinct classification of materials in the mid-twentieth century with the manufacturing of deliberately designed and engineered multiple composites. This concept of multiphase composites provides exciting opportunities for designing an exceedingly large variety of materials with property combinations that cannot be met by any of the monolithic conventional metal alloys, ceramics, and polymeric materials. Generally speaking, a composite is considered to be

any multiphase material that exhibits a significant proportion of properties of both constituent phases, i.e., matrix and reinforcement such that a better combination of properties can be realized. Composite materials are usually classified on the basis of physical or chemical nature of matrix phase, e.g., polymer-matrix composite-(PMC), metal-matrix composite (MMC), and ceramic-matrix composites (CMC) [1]. Among these composites, MMCs provide significantly enhanced properties such as higher strength, specific modulus, damping capacity, stiffness, good wear resistance, and weight savings [2]. Also, the growing requirement for advance materials in the area of aerospace and automotive industries had led to a rapid development of MMCs [3].

Metal matrix composites (MMC) are engineered combination of metal (matrix) and hard particles ceramics (reinforcement) to get tailored properties [4]. The aim involved in designing MMCs is to combine desirable attributes of a metal and ceramics. The addition of high strength, high modulus refractory particles to a ductile metal matrix produces a material whose mechanical properties are intermediate between the matrix alloy and ceramic reinforcement. Metals possess a unique set of properties such as high, strength, ductility, and high-temperature resistance but at the same time suffer from the low stiffness. On the other side, ceramics are stiff and strong but brittle. Aluminum and silicon carbide, for example, exhibit very different mechanical properties: Young's modulus of 70 and 400 GPa, coefficient of thermal expansion of 24×10^{-6}/°C and 4×10^{-6}/°C, and yield strength of 35 and 600 MPa, respectively. By combining these materials, e.g., Al 6061/SiC/17p (T6 condition), MMC with a Young's modulus of 96.6 GPa, and a yield strength of 510 MPa, can be produced [5].

Though fiber-reinforced MMCs offer excellent strength and modulus, their properties are not isotropic and are also very expensive. Lower cost and isotropy in properties have made discontinuously reinforced metal matrix composites (DRMMC) more attractive for a variety of commercial applications. DRMMCs have found their usage in aerospace applications, automotive industry, and several other areas of scientific and commercial interest [6]. In the recent past, a new class of DRMMC is developed in which two or more than two types of reinforcement particles are added into the matrix material for performance optimization. This class of DRMMC is called Hybrid MMC. Hybrid composite shows improved mechanical properties as compared to single reinforced MMC [7]. In general, there has always been a critical lack of research focus on exploring the effect of adding more than one reinforcement particles on properties of MMCs [7–9].

Various manufacturing processes for MMC have been developed in the past with the emergence of newer and advanced technologies. Some of the methods commonly used for production of discontinuously reinforced DRMMC are appended in Table 1, along with their comparative features [6].

Among various DRMMC fabrication processes, stir casting method is widely accepted and commercialized due to its simplicity, flexibility, and applicability to large production scale, which is usually not limited by shape and size of component to be fabricated [5]. Stir casting process for DRMMC is most economical to almost all of the available processes [6]. The cost of production through stir casting method is reported to be as low as one-third to half that of other fabrication methods, and for large production scale, cost reduces to one-tenth [10]. Stir casting route for fabrication provides the researcher an

Table 1 An overview of the different techniques used for DRMMC fabrication [6]

Method	Range of shapes and sizes	Metal yield	Range of vol. fraction	Damage to reinforcement	Cost
Liquid metallurgy (stir casting)	Wide range of shapes, larger size up to 500 kg	Very high (> 90%)	Up to 0.3	No damage	Least expensive
Squeeze casting	Limited by preform shapes, up to 2-cm height	Low	Up to 0.45	Severe damage	Moderately expensive
Powder metallurgy	Wide range, restricted size	High	–	Reinforcement fracture	Expensive
Spray casting	Limited shapes, large size	Medium	0.3–0.7	–	Expensive
Lanxide technique	Limited by preform shapes, restricted size	–	–	–	Expensive

opportunity to use wide range of reinforcement (up to 30%volume fraction) to enhance the properties [11, 12].

Hybrid MMCs are usually very hard and difficult to machine with the conventional machining processes owing to high tool wear rate and poor surface finish [8, 13]. Wire electric discharge machining could be a potential alternative for commercial machining of such materials as it is relatively free from the issues that are normally faced while machining with the conventional machining techniques. WEDM process removes the material by means of rapid, repetitive spark discharges from a pulsating direct-current power supply coupled with dielectric flow between the work piece and the tool [14]. Each discharge melts or vaporizes a small area of the work piece surface. This molten metal is then cooled in the dielectric fluid and solidifies into small spherical particles which are flushed away by the high-pressure dielectric fluid. However, the debris are not completely expelled from the machining zone due to narrower kerf and high spark frequency. The residual materials tend to resolidify to form a highly brittle layer on the outer surface of work piece, termed as recast layer. Additionally, generation of heat-affected zone (HAZ) and subsequently tensile residual stresses and micro-cracks has also been reported [15, 16], which usually leads to premature failure of the machined parts during the service life. Thickness of recast layer is largely depended on the parametric setting while machining with WEDM process [17]. The average thickness of recast layer while machining a low thermal conductivity material like pure titanium by WEDM process has been observed to be in a wide range of 6 to 58 μm, depending on the parametric setting employed for the purpose of cutting [18]. In general, the recast layer has been observed to increase with increase in pulse-on time and peak current [19–21]. Literature review suggests that the thickness of recast layer not only can be reduced by optimizing the WEDM process parameters but also it can be reduced by adopting trim cut strategy in which an initial rough cut is accomplished at high discharge energy level, followed by one or more than one pass of wire on the same path profile with an appropriate wire offset maintained at a reduced discharge energy level [22–27]. However, most of these investigations have missed on few critical issues such as proper screening of the parameters, first to rule out the insignificant parameters and to select the most important parameters for a systematic investigation of the trim cut operation, second to

fix the most appropriate levels/ranges for the selected variables that can help achieve the objectives of the trim cut operation, and third to establish the relation among the process variables and surface integrity features such as recast layer and micro-cracks density, particularly for machining of hybrid composite materials.

The present study is focused on fabrication of Al6061 matrix-based Hybrid MMC by stir casting process with varied amount of reinforcement particles, so as to study the effect of two different reinforcement particles (SiC and TiB_2) on the mechanical properties and microstructure, and, thereafter, machining by trim cut WEDM operation to investigate the effects of selected process parameters on machining characteristics and surface integrity features using fold over fractional factorial design (with resolution IV).

Experimental details

Fabrication of composites

Material for composites

For the present study, Al 6061(T6) alloy is selected as matrix material based on literature review and considering its superior mechanical properties, physical properties, and high workability, while SiC and TiB_2 are selected as reinforcement particles with the average grain size of 43 μm and 12 μm, respectively. Chemical composition of Al6061 (T6) alloy is presented in Table 2.

SiC having density 3.21 g/cm^3 is widely used as reinforcement owing to its superior mechanical properties, high wear resistance, wettability, and nonreactive property with Al alloy. TiB_2 is used as another reinforcement material for Hybrid MMC as it exhibits superior quality over ceramics like good thermal stability, low density (4.5 g/cm^3), and high hardness value (3400 HV). Reinforcement particles were supplied by M/S Parasmani Metals, Mumbai. The optimum grain size of particles is selected considering the effect of gravity and agglomeration of particles. Literature review reveals that grain size plays a very important role for deciding the properties of MMC. Coarser particles result in better distribution, while fine particles lead to agglomeration [28]; on the other side, larger particles have tendency to settle down at bottom, whereas smaller particles keep suspended in the molten matrix for a longer time which helps in effective pouring of melt in mold [29]. The grain size of SiC and TiB_2 were ascertained by using SEM at Central Research Facility (CRF), IIT Delhi. The SEM images of reinforcement particles are presented in Fig. 1a and b.

Fabrication technique

In the present study, stir casting process has been used to fabricate samples of Hybrid MMC with various proportions of reinforcement particles. Two-step melting technique (Fig. 2) has been used to get a uniform distribution of particles [30, 31]. Initially, the required amount of matrix material Al 6061 is placed in crucible of computer-controlled stir casting machine available at NIT, Kurukshetra. The temperature of furnace is raised to 750 °C which is more than the solidus of Al 6061 (650 °C) so as to get

Table 2 Chemical composition of aluminum 6061 alloy

Element	Si	Fe	Cu	Mn	Mg	Cr	Zn	Ti	Others	Al
Wt%	0.40–0.80	0.7	0.15–0.40	0.15	0.8–1.2	0.04–0.35	0.25	0.15	0.05	95.8–98.6

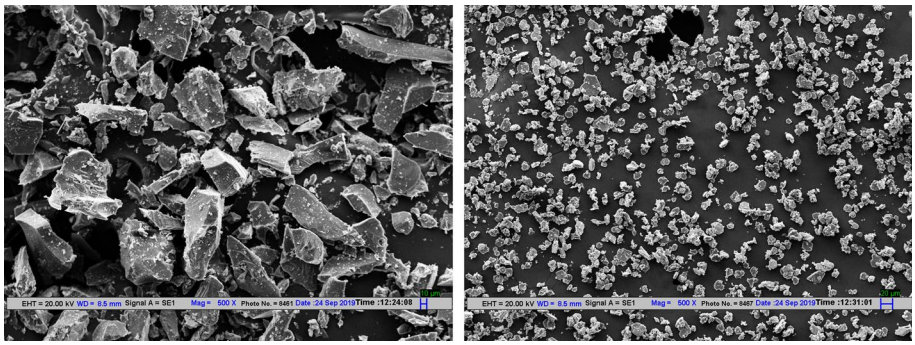

(a): SEM image of SiC particles (b): SEM image of TiB_2 particles

Fig. 1 **a** SEM image of SiC particles. **b** SEM image of TiB_2 particles

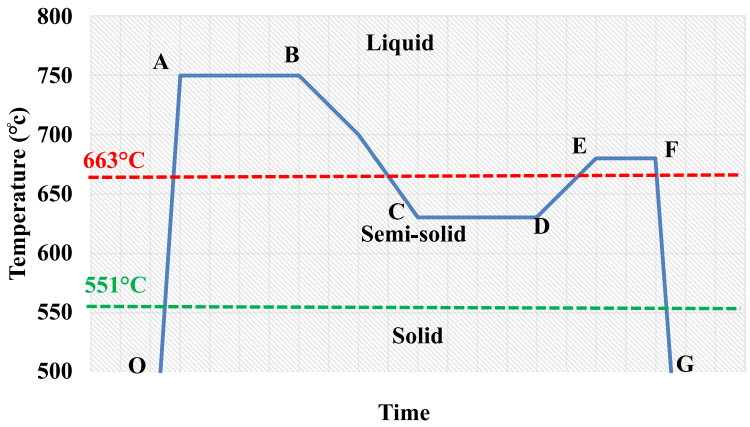

O-A: MELTING OF MATRIX MATERIAL, A-B: STIRRING TO FORM VORTEX , B-C: TEMP REDUCTION TO BRING IN SEMI-SOLID FORM AND ADDITION OF REINFORCEMENT PARTICLES, C-D: MIXING OF MATRIX AND REINFORCEMENT PARTICLES D-E: INCREASING TEMP TO BRING THE MELT IN LIUID FORM FOR POURING, E-F: HOLDING TIME, F-G: POURING AND SOLIDIFICATION

Fig. 2 Time and temperature graph

the complete melting of matrix material. Magnesium powder was used to increase the wettability between matrix melt and solid reinforcement materials. After complete melting, a four flat-bladed stirrer was inserted in the crucible to a depth equal to one-third of total height of melt from bottom of the crucible. Melt were stirred continuously (at 500 rpm) to achieve vortex formation; meanwhile, reinforcement particles of SiC and TiB_2 were preheated to a temperature of 200 °C in the inbuilt furnace of the machine. After vortex formation, reinforcement particles were added into crucible in the presence of inert gas (argon) with flow rate of 2 lpm. Thereafter, the temperature of melt was reduced to 630 °C, in between the liquidus and solidus temperature, so as to get the melt in marshy form to increase the viscosity of melt in order to achieve uniform distribution of particles. After mixing, the temperature of furnace is raised to 680 °C again so that the fluidity of melt increases. The complete mix was vacuum

poured into a preheated mold and allowed to solidify into required shape. A general functional sketch of stir casting process is shown in Fig. 3.

Selection of factors and their level

Literature review reveals that properties of the fabricated MMCs depend on a large number of factors, namely percentage composition of matrix and reinforcement particles, their size and shape, stirring speed, design and position of stirrer, particle incorporation method, and solidification method. In most of the research work reported on the subject, percentage composition of matrix and reinforcement materials is found to be most significant factor affecting the properties of fabricated composites. However, it is noticed that for Hybrid MMC, the volume fraction of one reinforcement material has been changed while keeping the volume fraction of the other reinforcement material fixed at a baseline. In these cases, there is a strong possibility of the confounding of the effect of total weight fraction of MMC and the effect of individual reinforcement particles. The present study is focused on assessment of the effect of weight percentage of SiC and TiB_2 reinforcement particles on the microstructure and mechanical properties of the hybrid MMC, by keeping the total weight percentage of reinforcement particles constant at 10%, so as to remove the confounding effect. Table 3 depicts the composition of reinforcement for the five samples fabricated, and the values of various fixed factors are appended in Table 4. The samples are illustrated in Fig. 4.

Characterization of composites

Microstructure of fabricated MMCs has been investigated by using optical microscopy and SEM, while tensile test and hardness test have been performed to investigate the mechanical properties.

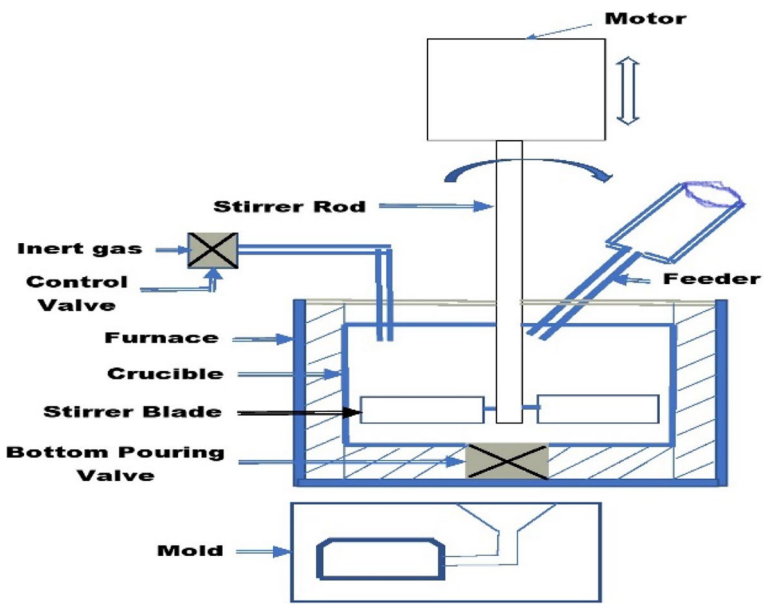

Fig. 3 Sketch of stir casting process

Table 3 Different compositions for fabrication of material

Sample no	% composition		
	Al6061	SiC	TiB_2
01	90	0	10
02	90	2.5	7.5
03	90	5	5
04	90	7.5	2.5
05	90	10	0

Table 4 Fixed parameters for stir casting

Parameter	Value
Stirring speed	500 rpm
Melting temperature	750 °C
Temp of melt during mixing	630 °C
Pouring temperature	680 °C
Wetting agent	Mg
Grain size of SiC particles	40–50 µm
Grain size of TiB_2	10–15 µm
SiC preheating temperature	200 °C
TiB_2 preheating temperature	200 °C
Position of stirrer in the melt	1/3 of melt height from bottom
Stirrer design	Four blade flat surface
Stirring time	10 min
Mould preheating temp	200 °C
Gas flow rate	2 lpm

Optical microscopy and SEM

Microstructure of fabricated Hybrid MMCs has been investigated by optical microscope (Olympus GX-53). Samples of 30 mm diameter and 10 mm thickness have been cut from the middle portion of fabricated MMCs, and thereafter, samples were mirror finished with double disc polishing machine with different grit sizes. After finishing, samples were etched properly in hydrofluoric acid (HF) solution for better investigation of microstructure and distribution of reinforcement particles into the matrix material. The prepared samples are shown in Fig. 5.

The optical micrographs of Al-SiC-TiB_2 composites with varied proportion of particles have been obtained at 400 ×. Figure 6 a–e shows the micrographs of Al6061-90%/TiB_2-10%, Al6061-90%/SiC-2.5%/TiB_2-7.5%, Al6061-90%/SiC-5%/TiB_2-5%, Al6061-90%/SiC-7.5%/TiB_2-2.5%, and Al6061-90%/SiC-10%, respectively. Figure 6 a and e shows the micrographs of MMC reinforced with single particles with 10%TiB_2 and SiC, respectively, whereas Fig. 6 b–d shows micrographs of hybrid composite reinforced with two types of particles, with composition varying from 2.5 to 7.5% while keeping the volume of matrix material fixed to 90%. Micrographs reveal that reinforcement particles are evenly distributed in all the samples. Microstructure of sample 1 (Fig. 6a) mainly contains primary α-Al dendrites, with eutectic phase

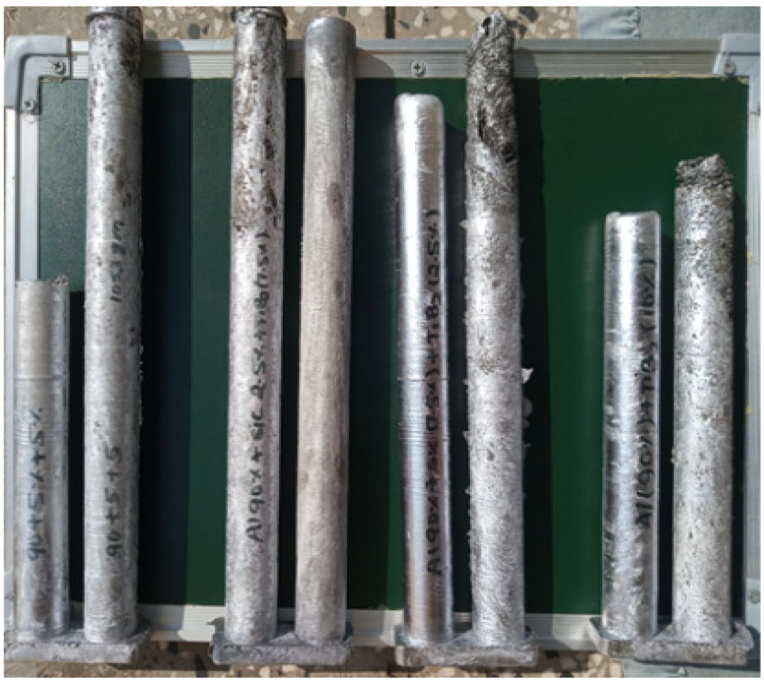

Fig. 4 Fabricated composites

Fig. 5 Sample for OM, SEM, and hardness test

of Al–Mg-Si [Al $(Mg)_5(Si)$] at grain boundaries, while TiB_2 is dispersed evenly on the surface. It also reveals the grains of α-Al are larger at few places and are without the reinforcement particles probably due to agglomeration of TiB_2 as observed from SEM image (Fig. 7b), owing to its lower grain size or settling of particles due to density difference. Sample No. 2 (Fig. 6b) exhibits better distribution of reinforcement particles resulting in improved mechanical properties. It is also observed for sample 2, dendritic structure of α-Al is broken into equiaxed structure, and uniform distribution of particles is achieved. The presence of SiC helps in avoiding agglomeration of TiB_2. It is observed from the micrographs that microstructure of hybrid composites (samples 2–4) is better than that of single reinforced MMC (samples 1, 5), in terms of grain size of the matrix material. With the increasing proportion

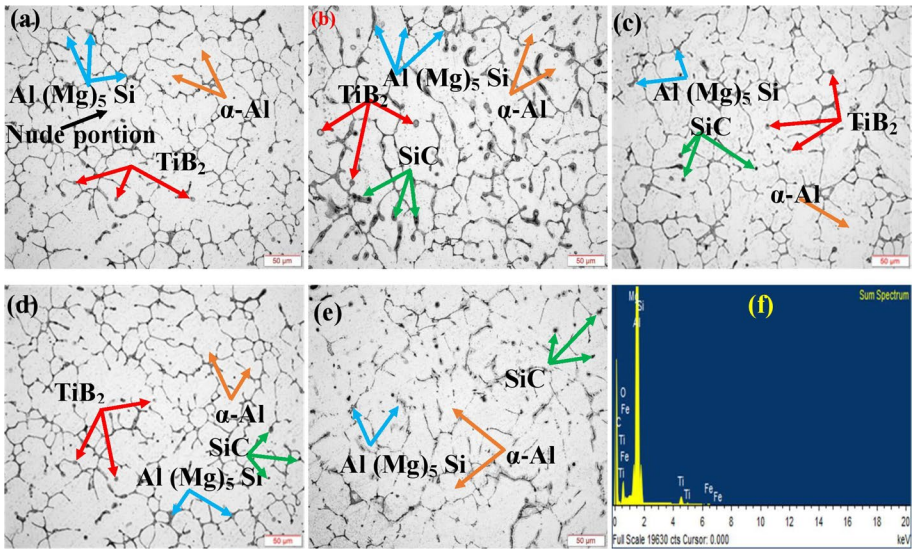

Fig. 6 Optical micrographs. **a** Sample 1. **b** Sample 2. **c** Sample 3. **d** Sample 4. **e** Sample 5. **f** EDS analysis

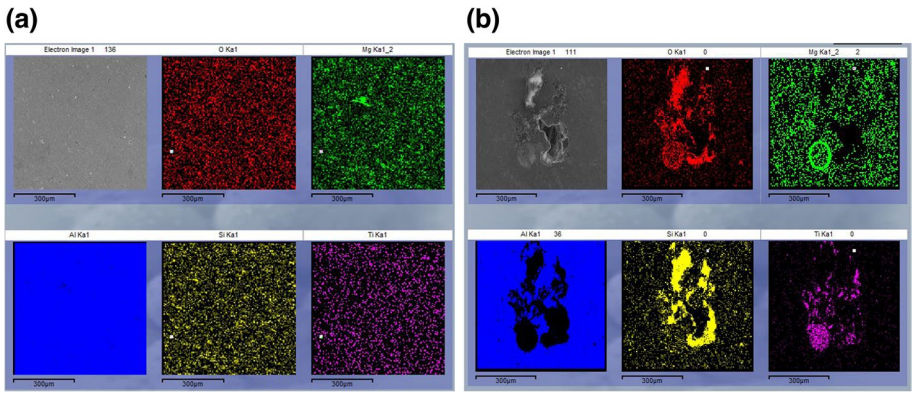

Fig. 7 **a** SEM sampling of Sample 2. **b** SEM sampling of Sample 1

of TiB_2, number of active grains is larger owing to its smaller grain size, i.e., 10–15 μm, which acts as nucleus for solidification, resulting in a greater number of grain boundaries and smaller size of grains. When compared to sample 1, sample 5 exhibits finer grains of matrix material because of the comparatively lower density and higher grain size of SiC than TiB_2 particles.

SEM sampling has been performed to ascertain the chemical composition of the fabricated composites. Figure 7a shows the SEM image of Sample No. 2, which illustrates the presence of added particles in to the matrix. It is also observed that reinforcement particles are uniformly distributed over the surface. Figure 7b shows the SEM image of Sample No. 1 in which agglomeration of TiB_2 is clearly visible. The EDS analysis of Sample No. 2 is shown in Fig. 6f, clearly indicating the presence of added reinforcement particles.

Tensile test

Tensile test has been carried out by using computer-controlled UTM machine (Biss UT-02–0100) having maximum load capacity of 100 KN. The specimen has been prepared as per ASTM E8 standard. The strain rate was kept at a value of 0.5 mm/min. Prepared samples and fractured samples after tensile test have been shown in Fig. 8a and b respectively. Stress–strain plots have been obtained automatically from the machine.

Tensile strength data of the tested samples is shown in Fig. 9a, in the form of bar graph. Stress–strain plots for all the samples which have been obtained from the UTM machine are shown in Fig. 9b–f. It is observed from the bar graph that the tensile strength of hybrid composites (Sample Nos. 2–4) is more than that of single reinforced composite (Sample Nos. 1, 5). It is also observed that among the hybrid composite, tensile strength increases with the increase in the composition of TiB_2. It is noticed that tensile strength of Al6061-90%/TiB_2-10% (Sample No. 1) is lower, attributed to agglomeration of particles which was observed in optical micrograph and SEM image shown in Fig. 7b. Tensile strength of Sample No. 2 is found to be highest owing to uniform distribution of reinforcement particles, smaller grains, and equiaxed structure of matrix material.

Hardness test

Vickers hardness test has been carried out on Vickers hardness tester (Wilson) load of 300 g. Hardness test was performed at 10 points, dispersed on the complete surface of each sample, and average value of these observations has been considered for analysis. The sample size of 10 was chosen to restrict the measurement error and the influence of noise factors. The samples prepared for optical microscopy have been used for hardness test.

Hardness test results are shown in Fig. 10 in the form of bar graph. The results follow the similar trend to the tensile test. The hardness value of hybrid composites is larger than that of single reinforced composite. Sample 2 exhibits the highest hardness value amongst the fabricated composites. It can be explained as a result of better distribution and wettability of particles with matrix material. Also, from the

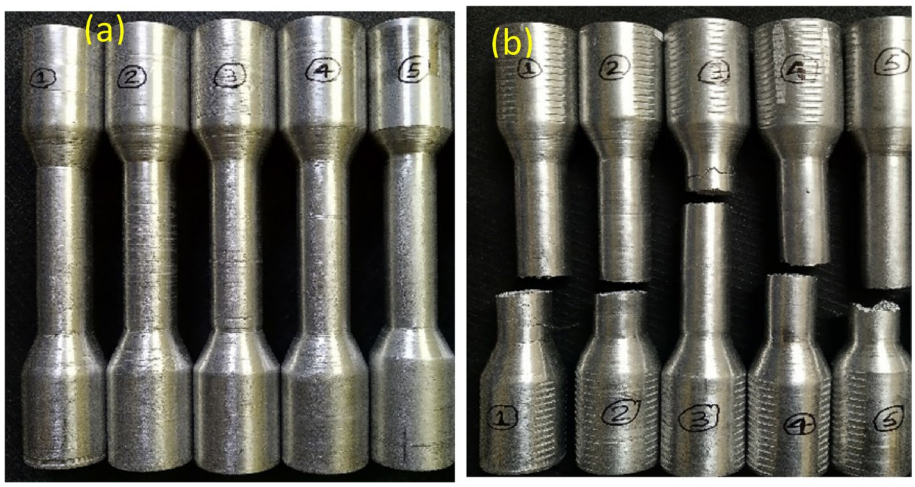

Fig. 8 Tensile test specimen **a** before test and **b** after test

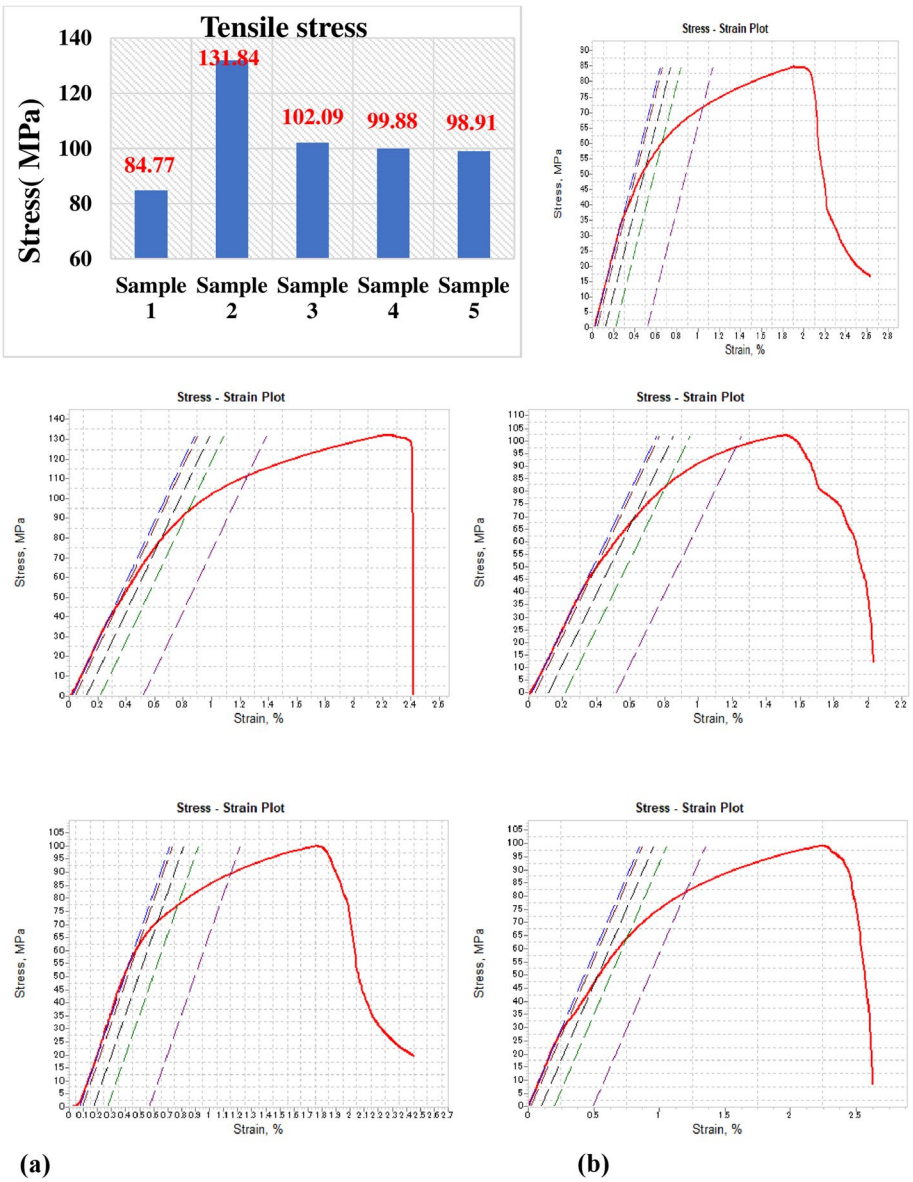

Fig. 9 **a** Tensile strength bar graph. **b** Stress–strain graph of Sample 1. **c** Stress–strain graph of Sample 2. **d** Stress–strain graph of Sample 3. **e** Stress–strain graph of Sample 4. **f** Stress–strain graph of Sample 5

micrographs, a greater number of grain boundaries can be observed (Fig. 6b), resulting in higher concentration of dislocations at the grain boundaries during solidification, increasing the hardness.

Machining of developed hybrid composite by WEDM process

Material and machine

For the present work, hybrid composite with composition Al6061-90%/SiC-2.5%/TiB_2-7.5% has been selected as work piece for machining by WEDM process as it exhibits superior mechanical and microstructural properties amongst the compositions fabricated. Work piece of size 75 mm × 27 mm × 9 mm is prepared as shown in Fig. 11.

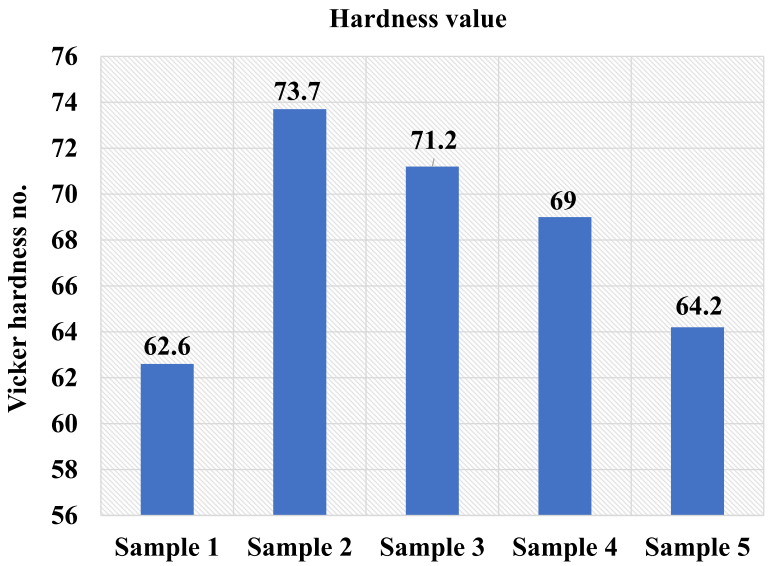

Fig. 10 Vickers's hardness graph

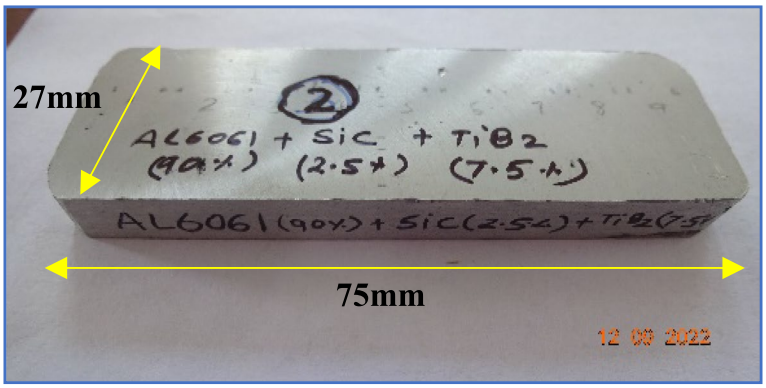

Fig. 11 Work piece for machining by WEDM

Machining experiments have been performed on Electronica Sprint cut (Electra-Elplus 40A DLX) CNC wire electric discharge machine (WEDM) to investigate the machining performance for trim cut operation. Cutting zone of WEDM process is illustrated in Fig. 12.

Methodology

Rough cut operation at high discharge energy condition has been performed followed by a trim cut at comparatively low discharge energy condition. NC program has been developed with parting length 1 mm and exit length 0.5 mm. Square punch of 5 mm side has been cut for each trial. During rough cut, 1 mm of the work piece has been left uncut to hold the sample in its position; thereafter, trim cut has been accomplished in the reverse direction with appropriate wire offset which was fixed through a pilot experiment. At the last, uncut portion of 1 mm was cut to separate the punch from workpiece. Path followed during rough, trim, and part cut is shown in Fig. 13.

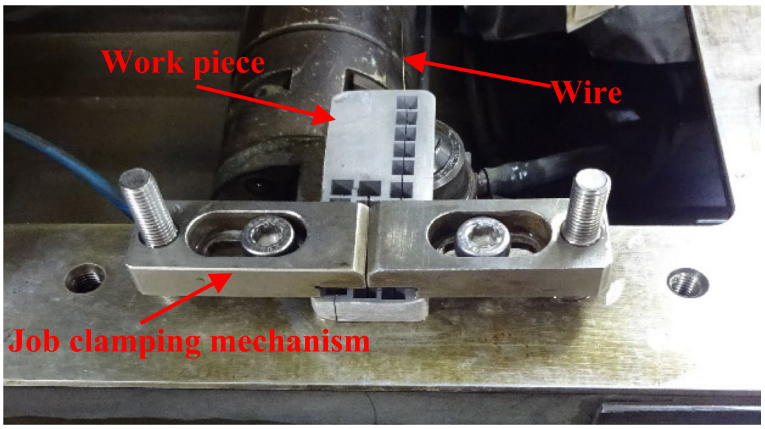

Fig. 12 Working zone of WEDM

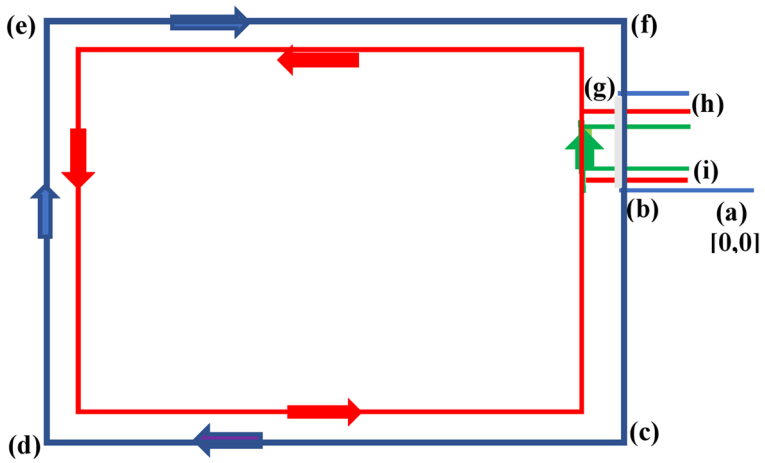

a-b: Entry length of wire, b-c-d-e-f-g-h: Rough cut path, h-g-f-e-d-c-b-i: Trim cut path , i-b-g-h: Parting path

Fig. 13 Rough, trim, and part cut strategy

Wire offset of 150 μm has been provided during rough cut so as to ensure cutting actually happens on the rough cut surface while performing trim cutting. If the offset is not provided during rough cut or inappropriately provided, there may be a considerably high probability of either no cutting or improper, nonuniform cutting during trim cut operation, and it will largely depend upon the value of spark gap for that particular experimental condition. Hence, it becomes highly important to first identify or fix a most appropriate value of wire offset, in conjunction with the actual spark gap for the particular experimental condition. The spark gap in turn depends on a number of factors governing the experimental condition such as work material properties, tool (wire) material and size, power-related parameters (pulse duration, current), and dielectric fluid pressure. Most of the studies reported on trim cut operation have not explained the rationale behind the appropriate selection of wire offset, which is the most critical parameter for trim cut operation. In the present study, the values of wire offset for

rough cut (150 µm) and trim cut (90 µm, 130 µm) have been arrived at after conducting three pilot experiments, first in rough cut mode at higher discharge energy condition followed by a trim cut at comparatively lower discharge energy condition. Spark gap was first assessed through these pilot experiments in order to fix the offset values mentioned above. The offset values for trim cut must be compatible with the offset value used in the rough cut to best serve the interests of the trim cut operation such as reduction of recast layer, improvement of surface finish, and reduction of micro-cracks. The concept of wire offset for rough and trim cut is illustrated in Fig. 14.

From a comprehensive literature review, it is realized that a number of WEDM process parameters have been reported to affect the responses of interest, and their judicial, logical, and proper choice or selection is mandatory to get the best results, particularly to achieve the objectives of the trim cut operation. In the present work, fold over fractional factorial design of resolution level IV has been used to investigate the parametric effects on the responses of interest during trim operation. Effects of seven factors, namely pulse on time (T_{on}), pulse off time (T_{off}), servo voltage (SV), peak current (I_p), flushing pressure (FP), wire tension (WT), and wire offset (WO), have been examined during trim cut operation. Table 5 presents the variable factors and their level during rough and trim cutting, whereas value of fixed parameters is appended in Table 6. Condition of wire breakage for rough cut condition has been ascertained through pilot experiments before deciding the levels of these parameters, and it was observed that wire breakage usually take place when the value of servo voltage and T_{off} was in close to 40 V and 40 MU (machine unit), respectively. Therefore, the minimum value for servo volt and T_{off} has been selected to 48 V and 48 MU, respectively. As per the general guidelines on the trim cut wire EDM operation, the energy-related parameters such as pulse on time and peak current are kept lower for

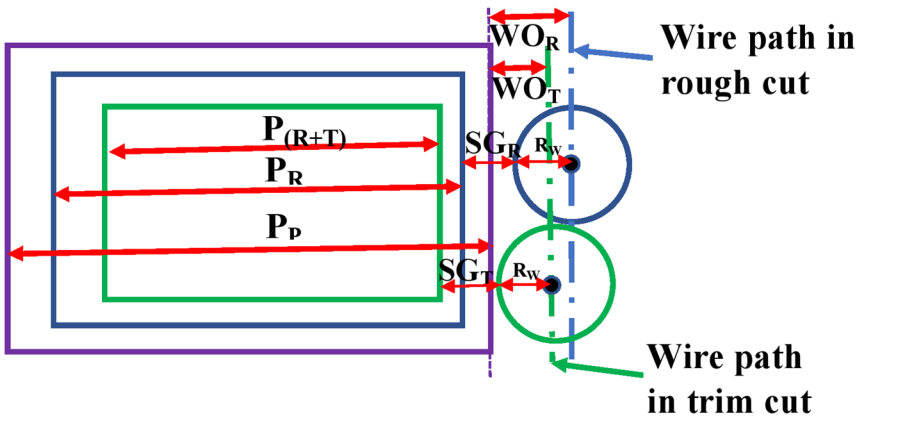

P_P: Programmed punch size, P_R: Punch size after rough cut, $P_{(R+T)}$: Punch size after rough+ trim cut, SG_R : Spark gap of rough cut, SG_T : Spark gap of trim cut, WO_R : Wire offset during rough cut, WO_T : Wire offset during trim cut, R_W : Wire radius

Fig. 14 Concept of wire offset during rough and trim cut

Table 5 WEDM parameters settings for rough and trim cut operation

Sl no	Process parameters	Symbol	Unit	Rough cut (machine unit/ actual unit)	Trim cut	
					Level 1 (machine unit/actual unit)	Level 2 (machine unit/actual unit)
1	Pulse on time	T_{on}	µs	128/1.5 µs	103/0.25 µs	115/0.85 µs
2	Pulse off time	T_{off}	µs	48/22 µs	40/14 µs	60/46 µs
3	Servo voltage	SV	V	48/48 V	60/60 V	90/90 V
4	Peak current	Ip	A	180/180 A	70/70 A	110/110 A
5	Flushing pressure	FP	–	High	Low	High
6	Wire tension	WT	g	8/1140 g	8/1140 g	11/1500 g
7	Wire offset	WO	µm	150/150 µm	90/90 µm	130/130 µm

Table 6 WEDM fixed parameters and their value

Process parameters	Unit	Rough cut	Trim cut
Open gap voltage	Volt	110 V	110 V
Electrode material	–	Soft brass (0.25 mmØ)	Soft brass (0.25 mmØ)
Dielectric fluid	–	De-ionized water	De-ionized water
Wire feed	m/min	8 m/min	6 m/min
Servo feed	–	2050	2050

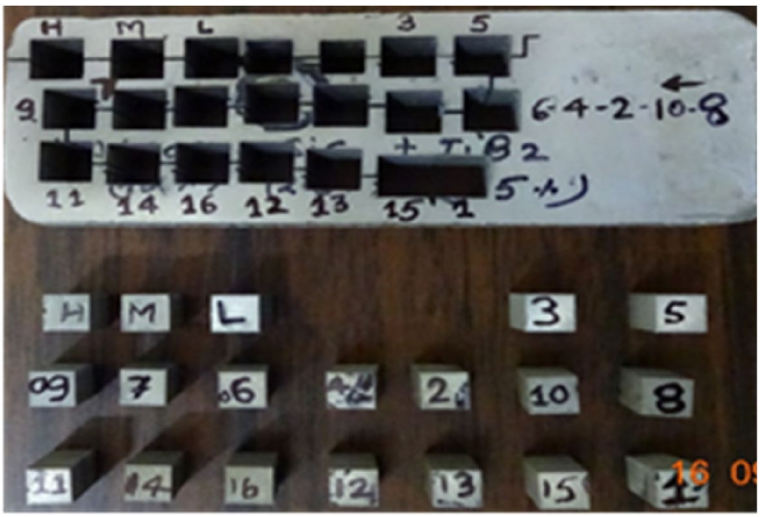

Fig. 15 Punch and work piece after machining

the trim cut operation, whereas wire tension and spark gap voltage or servo voltage are kept higher. The design of experiments has been formulated by using Minitab 16 software. Total sixteen trial conditions were executed, and 16 grooves of size 5 mm × 5 mm × 9 mm were cut from the work piece (Fig. 15). Additionally, one square punch of size 5 mm × 5 mm × 9 mm has been cut from the work piece at high discharge energy condition in rough cut mode only, so as to compare the values of the response characteristics obtained for the rough cut and trim cut modes.

Response variable for surface integrity

The advantage of trim cut strategy for improving surface integrity of WEDMed surface can only be fully realized if an optimum depth of layer is being removed during trim cutting. Cutting depth should not be more than the depth of actual recast layer thickness generated by the previous rough cut. To ensure this, wire offset must be selected appropriately so that the removal of the optimally thick layer can be achieved. Spark gap plays a very important role in selecting the appropriate wire offset during trim cut. It can be observed from Fig. 14 that actual size of punch after trim cut depends on the value of wire offset and spark gap for the specific trial condition. In the present study, spark gap has been recorded for each trial condition so that optimum value of wire offset can be determined for the further study. Calculation of spark gap has been done by using formula:

$$SG = \frac{[\mathrm{PP} - P(R+T)]}{2} + WO(Trim) - Wire\ radius$$

whereSG = Spark gapPP = Programmed size of punchP(R+T) = Punch size after rough and trim cutWO (trim) = Wire offset during trim cut

Dimension of punch has been measured by using Carl Zeiss (DuraMax) coordinate measuring machine (CMM) which has the accuracy of 2.5 µm. Figure 16 shows the working zone of CMM. On each surface of the punch, a plane is plotted by indenting the probe at six places, thereby getting 4 planes (Fig. 17), and one top plane was plotted in similar way for the perfect alignment of all four planes. Measurement of distance between two planes in *X*-axis and two planes on *Y*-axis was obtained. Average of these two observations has been considered for the measurement of spark gap.

Surface roughness is an important attribute of the surface integrity of machined surface. It has been measured by Surfcom 1400D surface roughness tester (Fig. 18b). The enlarged view of working zone is shown in Fig. 18c. Surface roughness (Ra value) has been measured at two places on three faces of the punch (Fig. 18a) in the transverse direction of machining and mean of the six observations has been considered for the analysis.

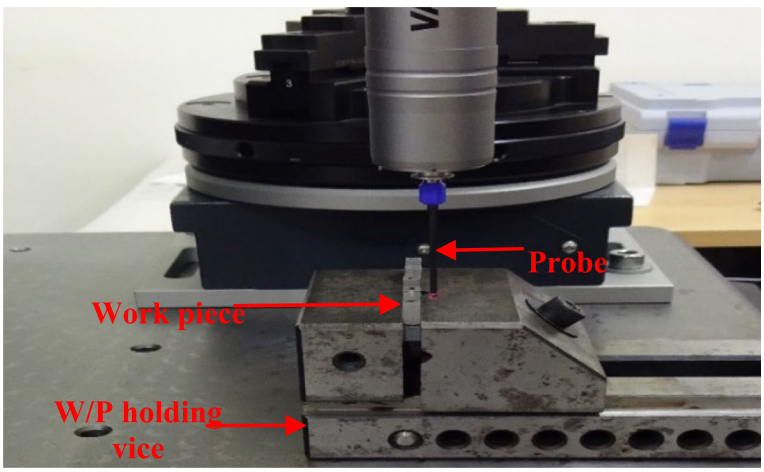

Fig. 16 Working zone of CMM

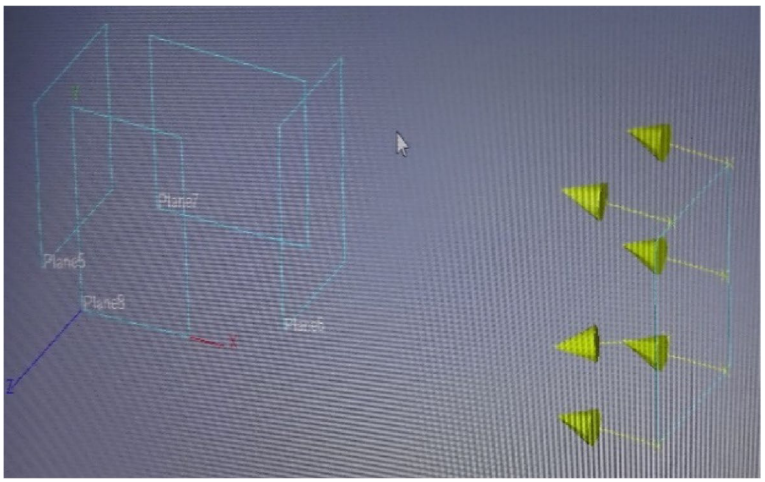

Fig. 17 Plane plotting in CMM

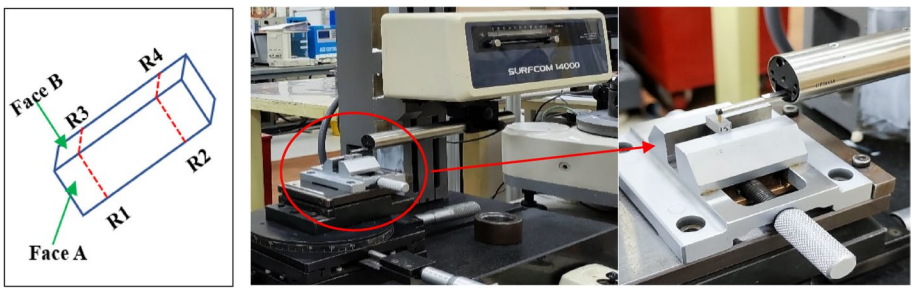

Fig. 18 **a** Surface roughness measurement technique. **b** Surfcom roughness tester. **c** Enlarged view of working zone of tester

Recast layer thickness has been measured for the selected specimen by using Hitachi (SU1510) Scanning Electron Microscope (SEM). After machining, samples were cleaned in ultrasonic cleaning machine and dried before etching in hydrofluoric acid (HF) solution. SEM image was obtained on each side, and average value of recast layer thickness is considered for the analysis.

Results and discussion

Evaluation of machining performance in trim cut operation

As per the path program for rough and trim cut operation (Fig. 13), initial rough cut at high discharge energy condition (T_{on}-128, T_{off}-48, SV-48, I_p-180A, FP-high, and WT-8) was performed, followed by trim cutting at various parametric settings mentioned in Table 7. The response characteristics, namely spark gap (SG) and surface roughness (SR) for all the experimental trials, have been measured and appended in Table 7. Recast layer (RL) thickness for selected samples has been computed as per the procedure mentioned in the "Response variable for surface integrity" section, and the values are appended in Table 8. Residual plots for spark gap and surface roughness have been drawn by using Minitab 16 software to check the adequacy of the data as well as the model, as shown in Figs. 19 and 20, respectively. From the normal probability plot, it can be observed

Table 7 Design of experiments (fold over fractional factorial) and the results obtained

Sample no	T_{on}	T_{off}	SV	I_p	FP	WT	WO	Punch size (mm)	Spark gap (μm)	Surface roughness (μm)
Rough cut	128	48	48	180	H	8	150	4.942	54	3.93
1	103	40	60	110	H	8	130	4.9401	34.95	3.46
2	115	40	60	70	H	11	90	4.882	24	3.39
3	103	60	60	70	L	11	130	4.9823	13.85	2.76
4	115	60	60	110	L	8	90	4.8781	25.95	3.56
5	103	40	90	110	L	11	130	4.9399	30.1	3.29
6	115	40	90	70	L	8	90	4.8798	30.05	3.01
7	103	60	90	70	H	8	90	4.8942	17.9	2.20
8	115	60	90	110	H	11	130	4.9278	41.1	3.38
9	115	60	90	70	L	11	90	4.8851	22.45	3.19
10	103	60	90	110	L	8	130	4.9398	35.1	3.38
11	115	40	90	110	H	8	90	4.8545	37.75	3.64
12	103	40	90	70	H	11	130	4.9448	32.6	3.05
13	115	60	60	70	H	8	130	4.932	39	3.20
14	103	60	60	110	H	11	90	4.9035	13.25	3.04
15	115	40	60	110	L	11	130	4.9436	33.2	3.22
16	103	40	60	70	L	8	90	4.9069	11.55	2.66

Table 8 Average value of recast layer

Sample no	T_{on}	T_{off}	SV	I_p	FP	WT	WO	RL (μm)	DE condition
Rough cut	128	48	48	180	H	8	150	24.6	–
2	115	40	60	70	H	11	90	16.9	MDE
8	115	60	90	110	H	11	130	18.1	HDE
11	115	40	90	110	H	8	90	20.6	HDE
12	103	40	90	70	H	11	130	11.2	LDE
13	115	60	60	70	H	8	130	13.5	MDE
16	103	40	60	70	L	8	90	9.79	LDE

that the residuals follow almost straight line, and actual values agree well with the predicted values. Residual versus fitted values plot illustrates the random scattering of the response data. Main effect plots for the spark gap and surface roughness are also obtained by using Minitab 16 software and shown in Figs. 21 and 23, respectively.

Effect of WEDM process parameters on spark gap

Figure 21 shows the main effect plots of the WEDM parameters for spark gap (SG). Peak current (I_p), pulse on time (T_{on}), wire offset (WO), and servo voltage (SV) are found to be the most significant; pulse off time (T_{off}) and fluid pressure (FP) are less significant, and wire tension (WT) is insignificant for spark gap (SG). Spark gap is mainly governed by the discharge energy condition of the machining process. It is observed that the main factors for discharge energy are pulse on time and peak current. In the present study, discharge energy condition has been categorized in three categories, namely high (HDE), medium (MDE), and low (LDE) discharge energy condition based on the value of T_{on}

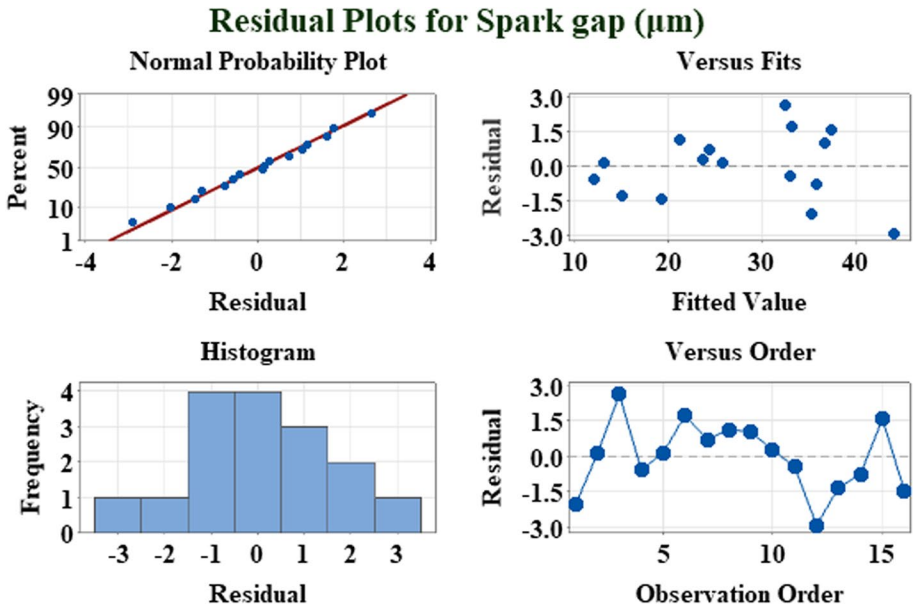

Fig. 19 Residual plots for spark gap

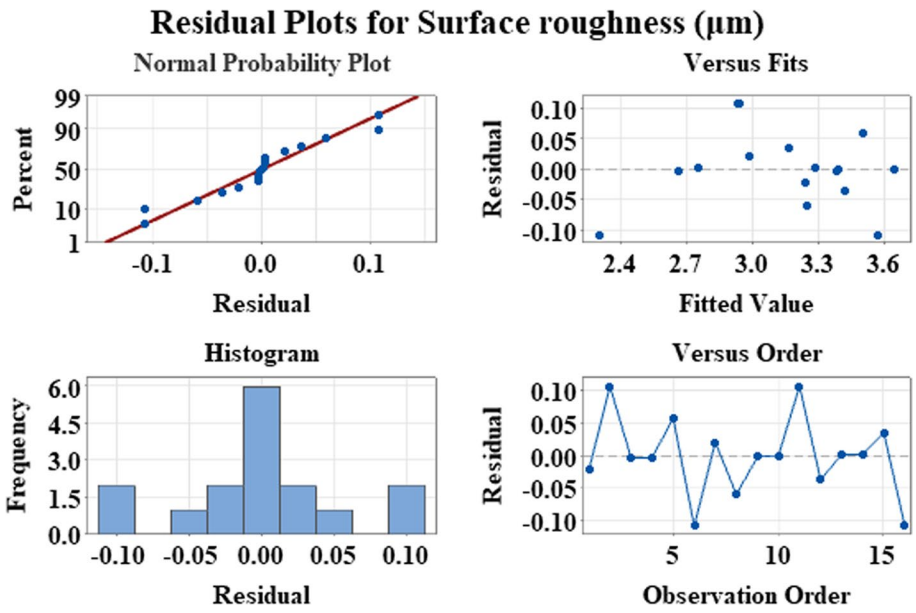

Fig. 20 Residual plots for surface roughness

and I_p. HDE trial conditions are those in which value of T_{on} and I_p is higher, MDE trial conditions are those in which one is set at higher side and other is at lower side, while LDE corresponds to the condition with both the factors are set at lower side. The average value of spark gap at HDE (Sample Nos. 4, 8, 11, and 15), MDE (Sample Nos. 1, 3, 5, 7, 10, 12, 14, and 16), and LDE (Sample Nos. 2, 6, 9, and 13) is found to be 34.5 µm, 28 µm, and 19 µm, respectively (Fig. 22). This value of spark gap can be used to determine the optimum value of wire offset in trim cut operation so that desired depth of material can be removed from the machined surface to improve surface integrity. It is also observed

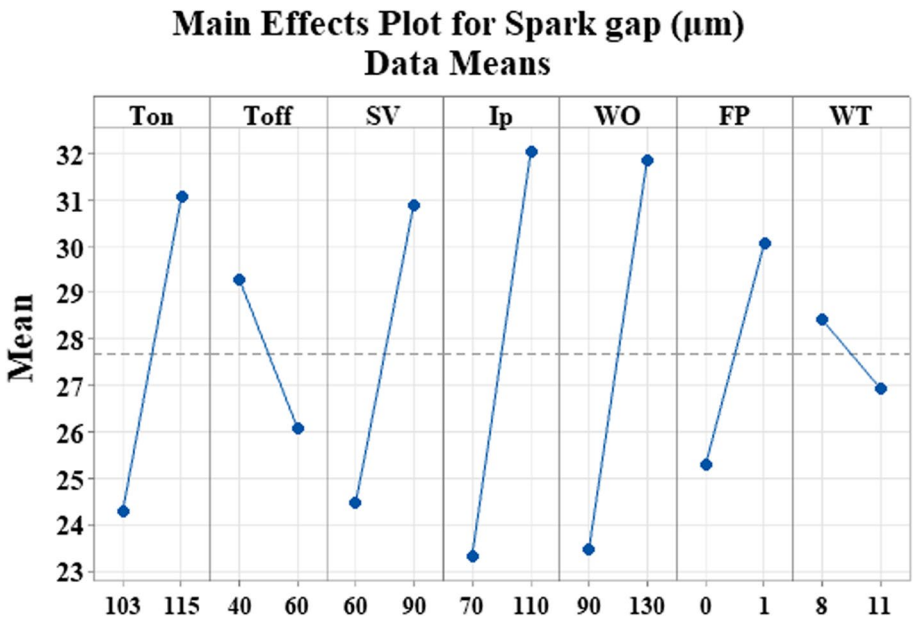

Fig. 21 Main effect plots for spark gap

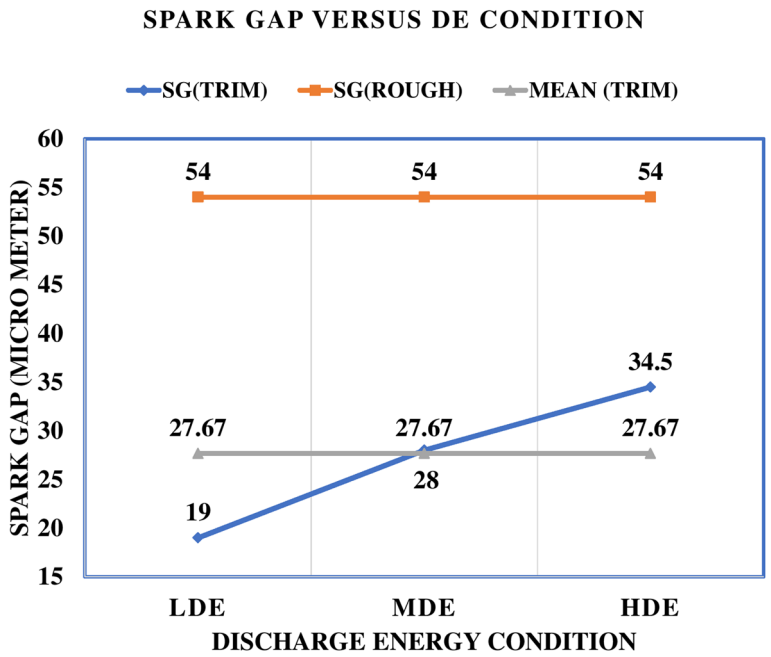

Fig. 22 Spark gap vs. discharge energy graph

that spark gap for HDE at trim cut (34.5 µm) is lesser as compared to rough cut, i.e., 54 µm (Table 7). The spark gap is found to increase with the increase in the wire offset. Average value of SG for lower and higher value of wire offset is found to be 22 µm and 33 µm, respectively. It is observed that for the same discharge energy condition, the spark gap value is higher for higher wire offset which is attributed to the free movement

of spark flow before actual removal of material from the work piece. Spark gap should increase with increase in servo voltage, as servo voltage maintains the gap between electrode and work piece which is conforming to the results obtained in the present study. The effect of fluid pressure on spark gap is found to be minimal; however, it is found that spark gap increases with increase in flushing pressure, and it is conforming to the concept that for the higher flushing pressure, debris removal from the gap will be more effective and leaving the gap wider. Wire tension has been found to be an insignificant factor for spark gap.

Effect of WEDM process parameters on surface roughness

Figure 23 shows the main effect plots of the WEDM parameters for surface roughness (SR). Peak current (I_p), pulse on time (T_{on}), and pulse off time (T_{off}) are found to be significant, whereas wire offset (WO), servo voltage (SV), fluid pressure (FP), and wire tension (WT) are insignificant for surface roughness (SR). Surface roughness (Ra) is the average distance between the ridge and valley formed on the surface. If discharge energy is higher, the material eroded from the substrate is of larger size, leaving behind larger craters on the surface. Similar to the spark gap, surface roughness is also found to be increasing with the discharge energy. The average value of surface roughness at HDE, MDE, and LDE is found to be 3.45 µm, 3.24 µm, and 2.67 µm, respectively (Fig. 24). It is observed that the maximum value of surface roughness in trim cut operation is 3.64 µm (Sample No. 11) which is lesser than the thickness of surface roughness after rough cut, i.e., 3.93 µm which proves that trim cut strategy helps in lowering the roughness. In the present study, minimum value of roughness recorded is 2.2 µm (Sample No. 7). Surface roughness decreases with increase in pulse off time, which is attributed as, with increase in T_{off}, spark frequency is reduced and a stable machining is performed which

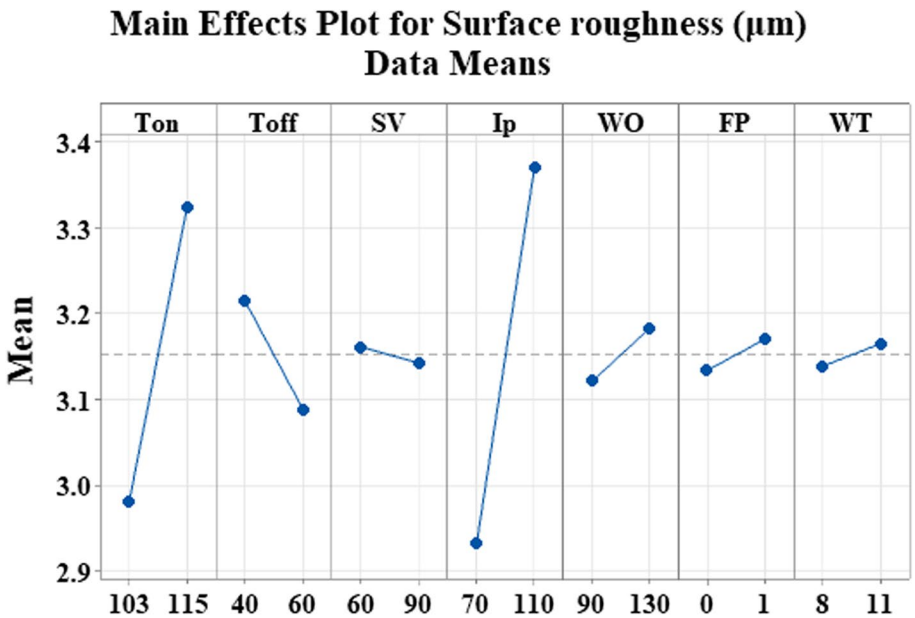

Fig. 23 Main effect plots for surface roughness

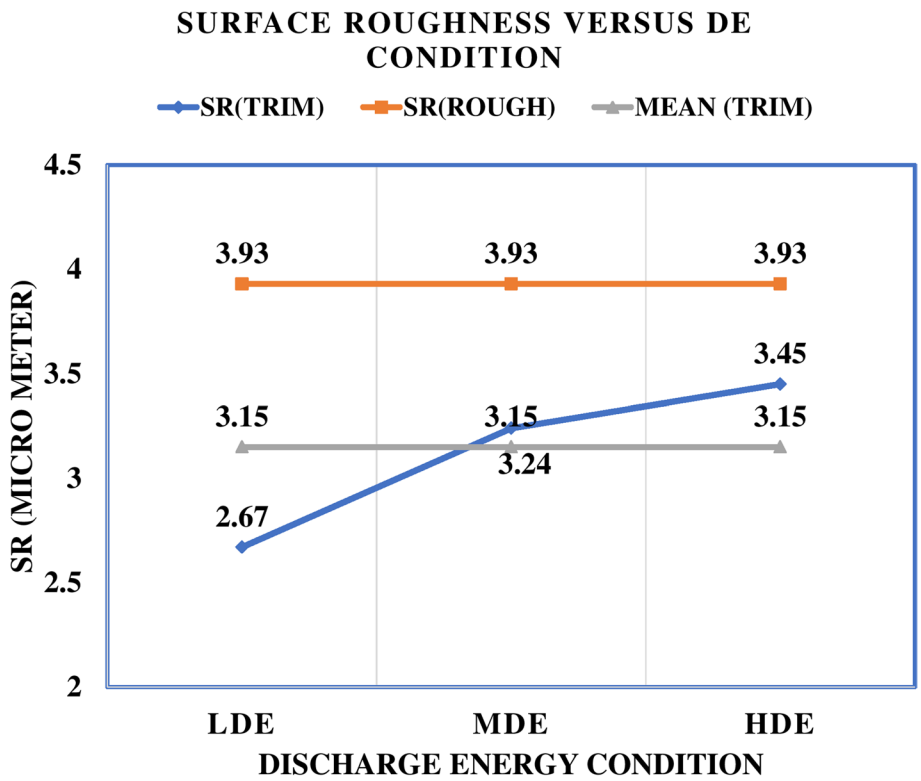

Fig. 24 Surface roughness vs. discharge energy graph

also provide ample amount of time for debris to be removed from the working zone leaving surface cleaner, and also, it reduces resolidification of eroded material.

Analysis of the recast layer and surface topography

Recast layer thickness for six selected trim cut samples and one rough cut sample has been measured by SEM at 1000 ×, and the values are appended in Table 8. Two samples from each of the discharge energy conditions namely, LDE, MDE, and HDE, were selected for SEM. The average value of recast layer after trim cut at HDE (Sample Nos. 8, 11), MDE (Sample Nos. 2 and 13), and LDE (Sample Nos. 12 and 16) is found to be 19.35 µm, 15.2 µm, and 10.5 µm, respectively, as shown in recast layer versus discharge energy condition graph (Fig. 25). The maximum value of RL is recorded for the rough cut (24.6 µm), whereas minimum value of recast layer is recorded for trim cut (Sample No. 12) at LDE condition (4.76 µm). Figures 26 and 27 show the SEM images of recast layer and surface texture for rough cut sample. The machined surface with rough cut condition consists of globules and larger size craters generated due to high discharge energy; however, no cracks are seen on the surface due to high conductivity of fabricated composites. It is also seen that eroded materials are resolidified all over the surface as recast layer having of variable thickness, which may affect the surface properties.

Figure 28a–c illustrates the SEM image of recast layer for trim cut operation at LDE (Sample No. 12), MDE (Sample No. 2), and HDE (Sample No. 11) condition respectively. Recast layer data (Table 8) suggests that trim cut strategy is an effective way

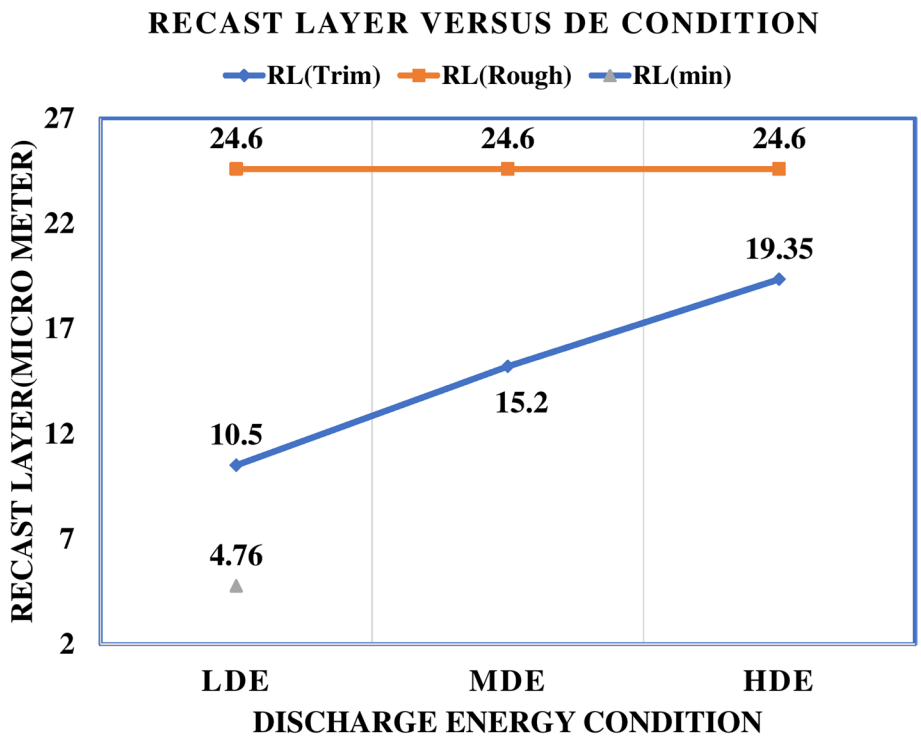

Fig. 25 Recast layer vs. discharge energy graph

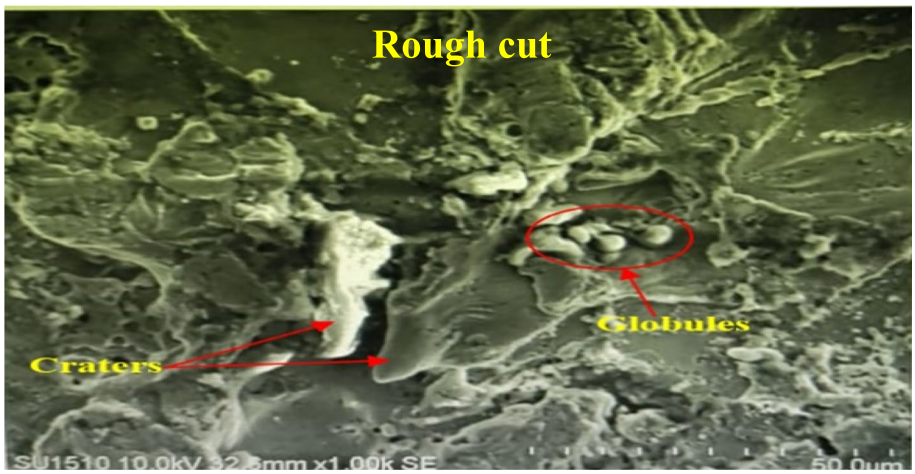

Fig. 26 Machined surface at rough cut condition

to improve the surface integrity of WEDMed surface by reducing the recast layer thickness. It is observed that thickness of recast layer is directly proportional to the discharge energy condition during trim cutting which depends on the parametric setting; thereby, it is envisaged that optimization of parametric setting plays an important role in improving surface integrity. Table 9 presents a comparative summary of the approach and the findings of this study with a previously reported study for the same work material (Al6061/SiC + TiB_2).

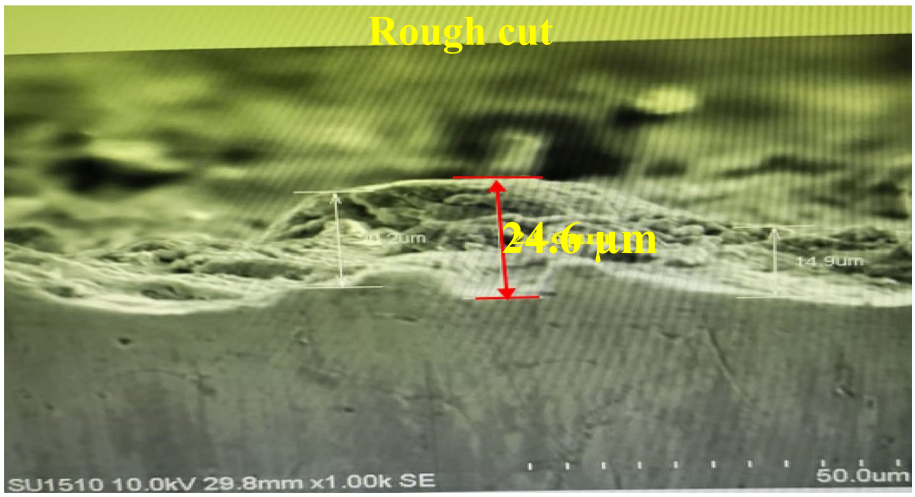

Fig. 27 Recast layer for rough cut sample

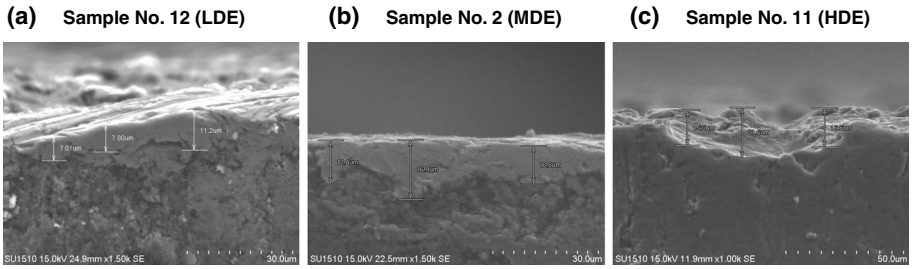

Fig. 28 Recast layer. **a** Sample No. 12. **b** Sample No. 2. **c** Sample No. 11

Conclusions

This study has been focused at fabrication of hybrid Al6061/SiC + TiB_2 composite with varied proportions of the two reinforcements, through stir casting route and the characterization of the fabricated samples, followed by a screening experiment (by using fold over fractional factorial design) to identify the significant parameters for trim cut WEDM operation of the composite material under different discharge energy conditions. The following conclusions may be drawn from the exhaustive experimental investigation performed through this study.

- Two-step melting technique has been found to be effective method for uniform distribution of reinforcement particles in to the melt, except for Sample No. 1 in which agglomeration of TiB_2 was observed due to larger density difference and smaller grain size of particles.
- Composite material with the composition Al6061-90%/SiC-2.5%/TiB_2-7.5% exhibits better mechanical properties (tensile strength 131.84 MPa and Vickers hardness value of 73.7 VHN) due to better distribution of particles and smaller grain size as confirmed through microstructure analysis.
- The mechanical properties of hybrid composites are found to be better than that of single reinforced composites. Also, it is found that mechanical properties

Table 9 A comparative summary of the findings/approach of the study

	Previous study Johny James. S. [8]	**Present study**
Fabrication of hybrid composite (Al6061/SiC + TiB_2)	Reported clustering of TiB_2 particles when it is kept at 5%, resulting in lower mechanical properties (i.e., tensile strength of 97.9 MPa)	In the present study, agglomeration of TiB_2 particles is observed when its concentration is increased to 10%; however, for the composite having 5% TiB_2, better mechanical properties have been obtained (i.e., tensile strength of 102 MPa). Two-step melting technique used in the present study resulted in better distribution of reinforcement particles
Selection of factors for trim operation for future study	Factors for trim cut WEDM operation have been selected based on the literature survey	A screening experimentation has been designed and performed to estimate the effect of WEDM parameters using fold over fractional factorial design
Improvement in surface quality and reduction in recast layer thickness	**Not reported**	Surface roughness is reduced to a value of 2.2 µm (from 3.93 µm), and recast layer has been limited to a value of 4.76 µm after performing trim cut operation
Selection of the levels/range for wire offset parameter	Value of wire offset in trim operation has been selected randomly	In the present study, value of spark gap is evaluated for trim cut operation at different parametric settings, so as to set the wire offset value judiciously to remove the required depth of material during trim cutting
Significant factors	**Not reported**	Peak current (Ip), pulse on time (Ton), wire offset (WO), and servo voltage (SV) have been found to be the most significant factors for spark gap while peak current (Ip), pulse on time (Ton), and pulse off time (Toff) were found to be significant for surface roughness

increase with increase in percentage composition of TiB_2 up to 7.5%, after which the agglomeration phenomenon degrades the properties.

- Trim cut strategy (for WEDM operation) has been found to be an effective way to improve surface integrity of the machined samples. Surface roughness is reduced to a value of 2.2 µm (from 3.93 µm), and recast layer has been limited to a value of 4.76 µm after performing trim cut.
- Peak current (I_p), pulse on time (T_{on}), wire offset (WO), and servo voltage (SV) have been found to be the most significant factors for spark gap, while peak current (I_p), pulse on time (T_{on}), and pulse off time (T_{off}) were found to be significant for surface roughness. The significant parameters may be included in the optimization experiment to be designed for investigation of the trim cut WEDM operation of hybrid composite.
- Spark gap evaluation for various parametric settings of the trim cut operation may be highly useful for selecting the optimum value of wire offset for the optimization experiment, so as to ensure that the most desired depth of material (recast layer) be removed from machined surface to improve the surface integrity.

Abbreviations

MMC	Metal matrix composite
WEDM	Wire electrical discharge machining
DRMMC	Discontinuously reinforced MMC
T_{on}	Pulse on time
Toff	Pulse off time
Ip	Peak current
SV	Servo voltage
WO	Wire offset
WT	Wire tension
FP	Flushing pressure
SG	Spark gap
HAZ	Heat-affected zone
lpm	Liter per minute

Acknowledgements
I acknowledge my heartiest feeling to my esteemed guide and all those who have directly or indirectly supported me in the present study.

Authors' contributions
Only one author with the help of course guide has done the literature survey, decided the objective of present study, carried out actual experimentation, analyzes the result, and written the paper.

Author information
The author is a Ph.D. research scholar of NIT, Kurukshetra, and serving in Indian Air Force since 28 Sep 2004 as a maintenance supervisor of a fighter aircraft.

Funding
Not applicable.

Availability of data and materials
The datasets are available from the corresponding author on reasonable request.

Declarations

Competing interests
The authors declare that they have no competing interests.

Received: 28 February 2023 Accepted: 20 September 2023
Published online: 04 October 2023

References

1. Surappa MK (2003) (2003) Aluminium matrix composites: challenges and opportunities. Sadhana 28(1–2):319–334
2. Sijo M T, K R Jayadevan (2016) Analysis of stir cast aluminium silicon carbide metal matrix composite: a comprehensive review. Proc Technol 24(2016):379–385
3. Himanshu Kala KKS, Mer SK (2014) A review on mechanical and tribological behaviors of stir cast aluminium matrix composites. Proceedia Mater Sci 2014(6):1951–1960
4. Singla M, Dwivedi DD, Singh L (2009) Chawla V (2009) Development of aluminium based silicon carbide particulate metal matrix composite. J Miner Mater Charact Eng 8(6):455
5. Hashim J, Looney L (1999) Hashmi MSJ (1999) Metal matrix composites: production by the stir casting method. J Mater Process Technol 92–93:1–7
6. Surappa MK (1997) Microstructure evolution during solidification of DRMMC: state of art. J Mater Process Technol 63:325–333
7. Vamsi Krishnaa M, Xavior AM (2014) An investigation on the mechanical properties of hybrid metal matrix composites. Proc Eng 97:918–924
8. Johny James S, Venkatesan K, Kuppan P, Ramanujam R (2014) Hybrid aluminium metal matrix composite reinforced with SiC and TiB_2. Proc Eng 97:1018–1026
9. Bodunrin MO, Alanemea K, Chown LH (2015) Aluminium matrix hybrid composites: a review of reinforcement philosophies; mechanical, corrosion and tribological characteristics. J Mater Res Technol 4(2):434–445
10. Skibo DM, Schuster DM, Jolla L (1988) Process for preparation of composite materials containing nonmetallic particles in a metallic matrix, and composite materials made thereby. US Patent No. 4 786 467.
11. Taha MA, El-Mahallawy NA (1998) Metal-matrix composites fabricated by pressure-assisted infiltration of loose ceramic powder. J Mater Process Technol 73(1998):139–146
12. Luo A (1995) Processing, microstructure and mechanical behavior of cast magnesium metal matrix composite. Metall Mater Trans A 26:2445
13. Lalmuan SK, Das S, Chandrasekarana M, Tamang SK (2017) Machining investigation on hybrid metal matrix composites- a review. Mater Today: Proc 4:8167–8175
14. Rebelo JC, Moroa Dias A, Kremer D, Lebrun JL (1998) Influence of EDM pulse energy on the surface integrity of martensitic steels. J Mater Process Technol 84:90–96

15. Hasçalýk A, Çaydas U (2004) Experimental study of wire electrical discharge machining of AISI D5 tool steel. J Mater Process Technol 148(2004):362–367
16. Kumar Anish, Kumar Vinod, Kumar Jatinder (2013) Metallographic analysis of pure titanium (grade-2) surface by wire electro discharge machining (WEDM). J Machin Manufact Automation 2(1):1–5
17. Lee HT, Tai TY (2003) Relationship between EDM parameters and surface crack formation. J Mater Process Technol 142:676–683
18. Kumar A, Kumar V, Kumar J (2013) Investigation of machining parameters and surface integrity in wire electric discharge machining of pure titanium. Proc IMechE Part B: J Eng Manufact 227(7):972–992
19. Wang C-C, Chowb H-M, Yang L-D, Chun-Te Lu (2008) Recast layer removal after electrical discharge machining via Taguchi analysis: a feasibility study. J Mater Process Technol 209(8):4134–4140
20. Newton TR, Melkote SN, Watkins TR, Trejo RM, Reister L (2009) Investigation of the effect of process parameters on the formation and characteristics of recast layer in wire-EDM of Inconel 718. Mater Sci Eng A 513–514:208–215
21. Kumar A, Kumar V, Kumar J (2014) Microstructure analysis and material transformation of pure titanium and tool wear surface after wire electric discharge machining process. Mach Sci Technol 18:47–77
22. Goswami A, Kumar J (2014) Investigation of surface integrity, material removal rate and wire wear ratio for WEDM of Nimonic 80A alloy using GRA and Taguchi method. Eng Sci Technol Int J 17(4):173–184
23. Chalisgaonkar R, Kumar J (2014) Multi-response optimization and modeling of trim cut WEDM operation of pure titanium (CPTi) considering multiple user's preferences. Eng Sci Technol Int J 1–10
24. A.B. Puri · B. Bhattacharyya Modeling, (2005) Modeling and analysis of white layer depth in a wire-cut EDM process through response surface methodology. Int J Adv Manuf Technol 2005(25):301–307
25. Sarkar S, Sekh M, Mitra S, Bhattacharyya B (2008) Modeling and optimization of wire electrical discharge machining of γ-TiAl in trim cutting operation. J Mater Process Technol 205(2008):376–387
26. Jangra KK (2015) An experimental study for multi-pass cutting operation in wire electrical discharge machining of WC-5.3% Co composite. Int J Adv Manuf Technol 76:971–982
27. Selvakumar G, Thiruppathi Kuttalingam KG, Ram Prakash S (2018) Investigation on machining and surface characteristics of AA5083 for cryogenic applications by adopting trim cut in WEDM. J Braz Soc Mech Sci Eng 40:267
28. Kok M (2005) Production and mechanical properties of Al_2O_3 particle-reinforced 2024 aluminium alloy composites. J Mater Process Technol 161(3):381–387
29. Thomas DG (1962) AIChE J 1:373
30. Khosravi H, Bakhshi H, Salahinejad E (2014) Effects of compo casting process parameters on microstructural characteristics and tensile properties of A356/SiCp composites. Trans Nonferrous Met Soc China 24(2014):2482–2488
31. Wang XJ, Wang NZ, Wang LY, Hu XS, Wu K, Wang YQ, Huang YD (2014) Processing, microstructure and mechanical properties of micro-SiC particles reinforced magnesium matrix composites fabricated by stir casting assisted by ultrasonic treatment processing. Mater Design 57:638–645

Publisher's Note